

CONF-95/036-7

# The Advanced Photon Source Event System\*

RECEIVED

JAN 11 1995

OSTI

The submitted manuscript has been authored by a contractor of the U. S. Government under contract No. W-31-109-ENG-38. Accordingly, the U. S. Government retains a nonexclusive, royalty-free license to publish or reproduce the published form of this contribution, or allow others to do so, for U. S. Government purposes.

Frank R. Lenkuszus and Robert Laird  
Argonne National Laboratory

## ABSTRACT

The Advanced Photon Source, like many other facilities, requires a means of transmitting timing information to distributed control system I/O controllers. The APS event system provides the means of distributing medium resolution/accuracy timing events throughout the facility. It consists of VME event generators and event receivers which are interconnected with 100Mbit/sec fiber optic links at distances of up to 650m in either a star or a daisy chain configuration. The systems event throughput rate is 10Mevents/sec with a peak-to-peak timing jitter down to 100ns depending on the source of the event. It is integrated into the EPICS-based APS control system through record and device support. Event generators broadcast timing events over fiber optic links to event receivers which are programmed to decode specific events. Event generators generate events in response to external inputs, from internal programmable event sequence RAMs, and from VME bus writes. The event receivers can be programmed to generate both pulse and set/reset level outputs to synchronize hardware, and to generate interrupts to initiate EPICS record processing. In addition, each event receiver contains a time stamp counter which is used to provide synchronized time stamps to EPICS records.

## INTRODUCTION

The Advanced Photon Source Event System provides a means of distributing medium resolution timing to distributed control system I/O controllers. A timing event is a numeric code broadcast over a fiber optic cable plant by event generators. An event generator can generate timing events in response to external inputs, from programmable internal sequence RAMs and upon command from the I/O controller processor. The numeric code is decoded and acted upon by event receivers located in the distributed I/O controllers. Event receivers, under software control, may generate hardware outputs and/or generate an interrupt to the I/O controller processor. Both the event generator and event receiver are A16/D16 single-width VME modules.

## GENERAL

A timing event is an 8-bit number that is broadcast over a cable plant. Since serial data transmission is used, a single fiber is sufficient to connect an event receiver to an event generator. Event generators may be cascaded to expand capability. Event receivers may be connected in either a star or a daisy chain configuration. There is, however, a limit to the number of event receivers that can be daisy chained since the serial bit stream out of a receiver is not decoded and regenerated but merely repeated through a buffer/driver. Figure 1 shows an example of how event generators and event receivers may be interconnected.

The event system uses the TAXIchip<sup>TM</sup> (Transparent Asynchronous Transmitter/Receiver Interface [1] to provide serial links between event generators and event receivers. The TAXIchips provide the parallel-to-serial, serial-to-parallel conversions and link management functions. The serial links run at 100Mbits/sec, but since an 8-bit event is encapsulated in a 10-bit packet, the maximum event transfer rate is 10Mevents/sec. Our tests show the system works reliably at distances of 650m. We have not tested longer link lengths.

## THE EVENT GENERATOR

The event generator is a single-width VME module which generates timing events in response to several stimuli. Figure 2 shows a simplified block diagram of the event generator. A 10MHz oscillator sets the TAXI transmitter's operating frequency. The TAXI transmitter multiplies the operating frequency by a factor of 10 to create the 100MHz bit rate. The buffered 10MHz clock output of the TAXI transmitter is used as the clock for the event generator's synchronous internal logic.

Events are generated in response to external inputs, sequence RAM contents, and register writes from the VME bus. In addition, a fiber-optic input is provided which accepts the output of an upstream event generator and is used to cascade event generators. Each potential source of events has an independent enable/disable control.

Eight edge-triggered maskable inputs are provided. Each of these inputs has an associated mapping register which is loaded with the event code to be generated upon receipt of the input.

Two 32k event sequence RAMs are included. Each sequence RAM accepts an external clock and external start. The external clock rate, 1MHz maximum, determines the time resolution and maximum time duration of an event sequence. Upon receipt of the external trigger, the sequence RAM is stepped through sequentially at the external clock rate. The contents of each location may contain an event code. Non-null codes (contents not equal to "0") are transmitted and the null code, 0, is ignored. The time interval between the start input and a generated event code is determined by the clock rate and the RAM address at which the event code is stored. A reserved code, the "end sequence" event code, may be placed in the RAM to define the end of the sequence. Another reserved code, the "freeze sequence" code, when encountered, will cause the sequence to suspend. The sequence will resume upon receipt of another "start." Neither the "end sequence" nor the "freeze sequence" codes are transmitted.

MASTER

\*Work supported by U.S. Department of Energy Office of Basic Energy Science under Contract No. W-31-109-ENG-38

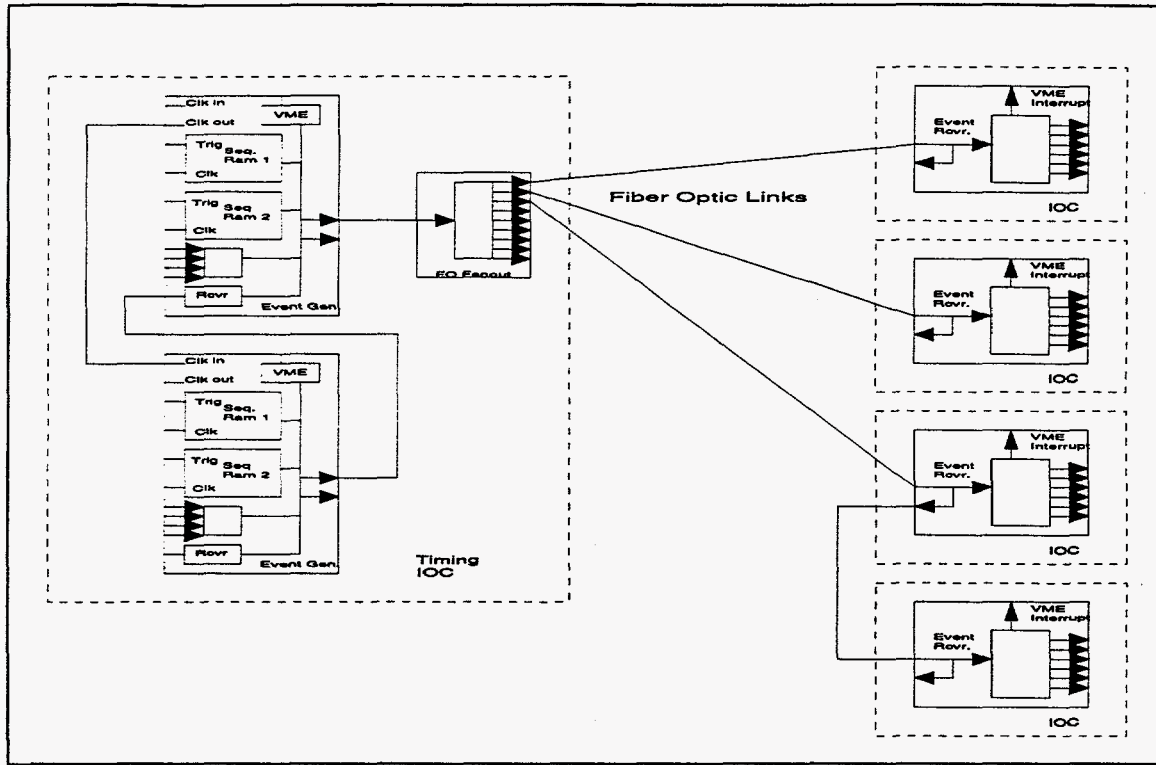


Figure 1 Example Event System Interconnection

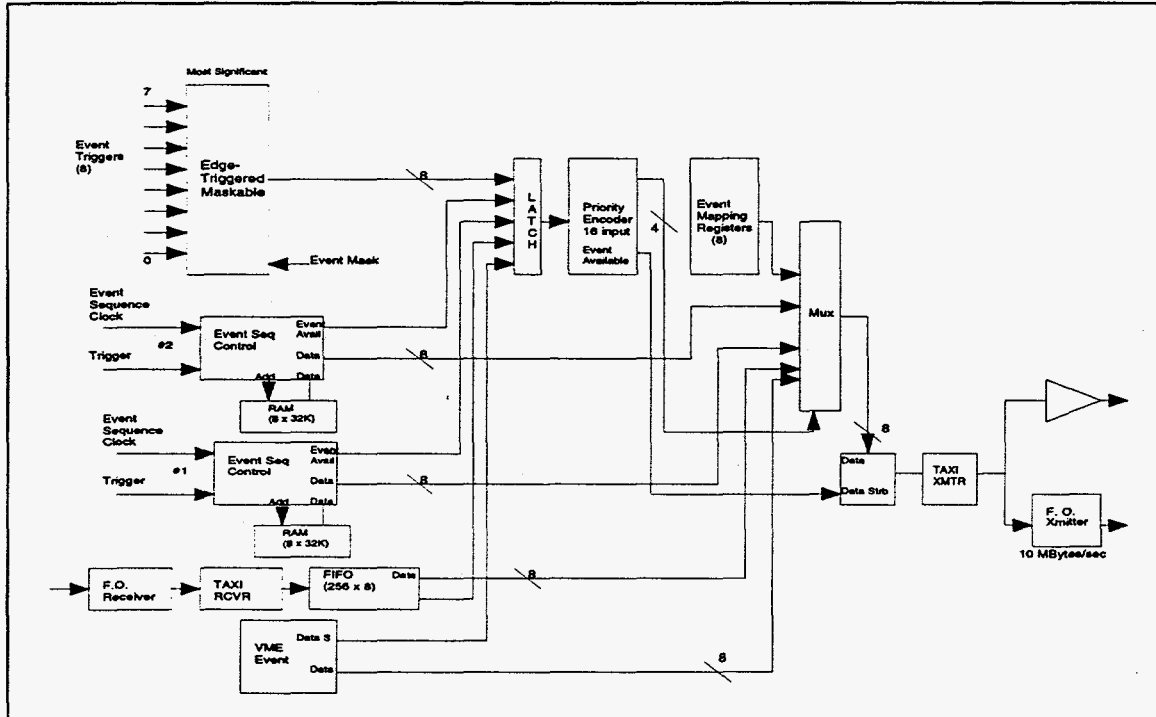


Figure 2 Event Generator Block Diagram

Each event sequence may be placed in one of four modes: normal, single sequence, recycle sequence, and alternate. In normal mode, the sequence is executed once for each start. In the single sequence mode, the sequence is executed once upon receipt of a start. Upon completion of the sequence, the sequence enable bit is reset, causing subsequent starts to be ignored. The recycle mode

causes the sequence to continuously repeat after receipt of an initial start. The alternate mode connects the start and clock of sequence RAM 2 to the respective inputs of sequence RAM 1 so that both sequence RAMs receive a common clock and a common start. The two sequence RAMs are used in a foreground/background mode. The background RAM sequence may be modified, while the foreground RAM generates the sequence. The role of the two RAMs is then switched between the end of the sequence and the next start. Thus, in this mode, seamless timing changes may be made to the event sequence. In fact, a software slider can be attached to an event code and used to move the event code's time of occurrence. As the slider is moved, the background RAM is updated with a new position for the event and switched to the foreground. The two RAMs "alternate" between foreground and background as the slider is moved.

Each event RAM is randomly addressable via its own address register. An auto increment control bit is provided for each of the address registers. When this bit is set, the address register is automatically incremented upon each VME access. Conversely, if the bit is reset, the address register is not incremented on each VME memory access. A null fill command is provided for each of the RAMs which zeros the entire RAM. The event generator has an on-board lithium battery which preserves RAM contents on power down.

In practice, the RAMs tend to be sparsely filled. Our worse case to date is 15 event codes in a sequence. We considered using a scheme based on storing delta time/event code pairs, but felt that the additional hardware and software complication was not worth any potential benefit.

The third way to generate an event code is via a VME write of an event code to the VME event register. The value written to this register will be transmitted as an event code. An example use of this method is the event system heartbeat. The heartbeat event, another reserved event code, is used by the event system to verify operation and link continuity. The heartbeat event is generated by the VME processor periodically writing the heartbeat event code to the VME event register.

A fiber optic input is provided to receive the serial event code stream from other additional event generators. This provides the mechanism for cascading event generators. The incoming event stream is converted to an 8-bit byte by a TAXI receiver. Received event codes are queued in a 256-deep fifo stack for retransmission. Through this mechanism the event streams of multiple event generators are combined into a single event stream. The TAXI receiver is phase locked to the upstream TAXI transmitter. Thus, since the onboard TAXI transmitter uses its local oscillator for its time base, the onboard TAXI receiver and onboard transmitter are not normally phase locked. As a result, an additional peak-to-peak jitter of 100ns is incurred for each unsynchronized event generator that an event passes through. For event generators in close physical proximity, this jitter can be eliminated by driving the TAXI transmitter clock on each "slave" from the clock of a "master." The event generator has a front panel clock input and clock output to permit multiple event generators to be run synchronously.

Since events are generated from multiple asynchronous sources, collisions will occur. The event generator uses a priority encoder to resolve collisions. The order of priority with highest first is: externally triggered events, RAM sequence 1, RAM sequence 2, TAXI receiver, VME-generated events. A collision causes the lower priority event to be delayed by up to 100ns to allow the higher priority event to complete transmission.

## THE EVENT RECEIVER

The event receiver, a single-width VME module, receives the serial event stream over a fiber optic cable. A simplified block diagram is shown in Figure 3. The event stream is buffered and retransmitted via a fiber optic transmitter. This output may be used to cascade event receivers. The on-board TAXI receiver converts the serial event stream to an 8-bit parallel stream.

The event receiver has fourteen 100ns-pulse outputs, seven set/reset flipflop outputs, and four programmable delayed-pulse outputs. The delayed-pulse outputs offer programmable delay or width of up to 1.6 seconds. The actual range of programmable delay and width of a channel depends on which of three different versions of the delay generator PLD is socketed for that channel. Any and all of these outputs may be generated upon receipt of any event code. In addition, the event receiver may generate a VME interrupt in response to any event. The response of the event receiver to a particular event is determined by a mapping RAM that maps event codes into responses.

Incoming events are applied to the address lines of two 16-bit by 256 word mapping RAMs. The contents of the location corresponding to an event code determines what action will be taken by the event receiver upon receipt of that event code. Only one mapping RAM is active at a time. The inactive RAM may be modified and then selected as the active RAM. This permits bumpless modification of the mapping RAM on a running system. Both RAMs are battery backed up with an on-board lithium battery.

The format of the mapping RAM is shown in Figure 4. The 14 least significant bits determine what hardware outputs will be generated upon receipt of an event. The bits are multi-functioned. For example, setting bit 1 in the map location for a particular event code can cause the 100ns-pulse output number 1 to be generated, set flip-flop number 1, and/or trigger delay pulse output number 1. Each of the outputs has an enable/disable bit. Which output(s) will be generated when the event is received depends on the state of the enable bits. In this case, if the 100ns-pulse output number 1 is disabled, and flip-flop number 0 is disabled, but delayed-pulse number 1 output is enabled, the delayed-pulse output but neither the flipflop nor the 100ns-pulse outputs will be generated when this particular event is received. The set/reset of the seven flipflops are controlled by odd/even pairs of mapping RAM bits. Since there are only four delayed-pulse outputs available, only the four least significant bits of the mapping RAM are used to control delayed-pulse outputs.

The event receiver provides hardware to support synchronized time stamps. Two reserved event codes are decoded internally to control the time stamp counter: an increment time stamp counter code and a reset time stamp counter code. Upon receipt of the reset time stamp counter code, all event receivers reset their time stamp counters. Similarly, upon receipt of an increment time stamp counter event code, all event receivers advance their time stamp counters by one. Thus all event receivers (assuming they are all downstream of the event generator issuing the time stamp events) maintain a synchronized relative time stamp which may be read via VME. We presently are using a 1kHz clock to generate the increment time stamp event. The time stamp counter may be incremented by a 1MHz internal clock derived from the TAXI receiver's clock instead of the increment time stamp event. Since all the TAXI receivers are phase locked to the incoming bit stream clock, the 1MHz clocks of all event receivers are phase locked.

As mentioned earlier, each event can cause a VME interrupt to be generated. The most significant bit in the mapping RAM location for a particular event code determines if an interrupt is generated. If that bit is set for a particular event code, upon receipt of that event an interrupt is generated and the event code and the 24 least significant bits of the time stamp counter are placed in a 32-bit by 256-word event/time fifo. The interrupt service routine reads the fifo to determine the number of the event generating the interrupt and the value of the time stamp counter when that event occurred.

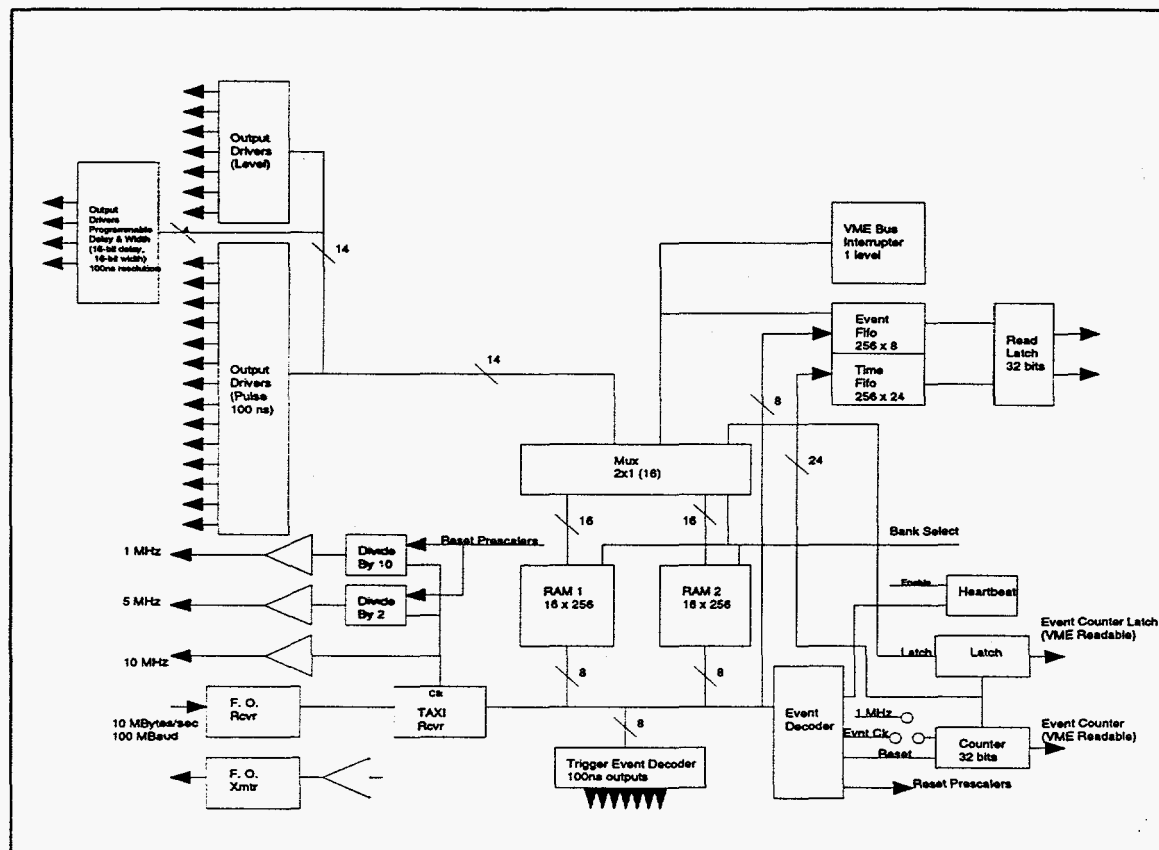


**Figure 3 Event Receiver Block Diagram**

In addition to generating an interrupt or generating outputs, an event may cause the current value of the time stamp counter to be latched in a VME-readable 32-bit latch. We have not made use of this feature to date.

The event receiver provides three frequency outputs: 10MHz, 5MHz, and 1MHz. These frequencies are derived from the TAXI clock which, as mentioned previously, is phase locked to the incoming bit stream. The 5MHz and 1MHz frequencies are generated from the 10MHz TAXI clock by synchronous counters. A reserved event code, the “reset event receiver prescalers” event code, causes the prescalers to synchronously reset. Thus the three frequency outputs are phased the same across all receivers. There will, however, be time skew due to differing propagation delays resulting from different signal path lengths.

15	14	13	12	11	10	09	08	07	06	05	04	03	02	01	00
VME Interrupt	Latch Time	Pulse 13 Set FF 6	Pulse 12 Reset FF 6	Pulse 11 Set FF 5	Pulse 10 Reset FF 5	Pulse 9 Set FF 4	Pulse 8 Reset FF 4	Pulse 7 Set FF 3	Pulse 6 Reset FF 3	Pulse 5 Set FF 2	Pulse 4 Reset FF 2	Pulse 3 Set FF 1	Pulse 2 Reset FF 1	Pulse 1 Set FF 0	Pulse 0 Reset FF 0

Figure 4 Event Receiver Mapping Ram Data Format

The module can generate VME interrupts for event received, heartbeat missed, event fifo full, and TAXI receiver error.

## EXPERIENCE AND USE

The first event receivers and generators were installed in the APS control system in January of 1994. Presently, we have 52 event receivers and 6 event generators in use. We have not experienced any hardware failures to date. A test was run over a seven-day period, transmitting and receiving an event at 250kHz over a 625m fiber optic cable. No errors were detected before the test was terminated. The event was transmitted and received over 150E9 times without error. Another test involved using the time stamp counters to verify event system reliability. This test was run on the installed system which had its normal event traffic. The time stamp counters in four event receivers were reset (with the reset time stamp counter event code) and allowed to accumulate time stamp events. The time stamp event was generated at 1kHz. The test was terminated after approximately 90 hours of running time. The time stamp counters of each of the four event receivers agreed to the tic (326,187,516 tics to be exact). While these tests are not rigorous, we believe that the system reliably transmits and receives events.

Presently, the APS event system uses 37 of the 255 possible event codes. The event rate is approximately 5.2k events/sec. The bulk of that rate is due to two sources: the 1kHz time stamp event and a 4kHz orbit feedback synchronization clock.

The hardware outputs have proved useful for a number of different purposes. They have been particularly useful for quickly providing timing for a new or unforeseen application. In most instances, a properly timed event was already available, so all that needed to be done was to program the appropriate event receiver's mapping RAM to generate the desired type of output. No cable pulling or termination was required.

The event receiver and generator are fully supported under EPICS. Five record types are available for use with the event system. The event generator record provides the basic interface to the module. Event generator RAM records provide the means to program the event sequence RAMs. The event receiver is controlled through its own record type with an additional record type to specify mapping RAM contents. The fifth record type available is the standard EPICS event record. This record has proven to be extremely useful for synchronizing database record processing with external processes. The event record provides the mechanism for triggering record processing upon receipt of an event. The event receiver is programmed via an event receiver RAM record to generate an interrupt upon receipt of the desired event. The EPICS event record is set to process upon an I/O interrupt with the desired event. Under these conditions, the EPICS driver causes the event record to process upon receipt of the desired event. Any desired set of database records can then be caused to process through the EPICS forward link mechanism.

The synchronized time stamps are also fully supported under EPICS. Three modes are available for time stamping the processing of an EPICS record when the event system is used. Under the "normal" mode, the record's time stamp is obtained from the VME processor's 60Hz clock. In this mode, the time stamps across multiple processors will be within one tic of 60Hz. The second mode is the "event" mode. In this mode, a record's time stamp is the last time of occurrence of a selected timing event. The third mode is the high resolution mode wherein the record obtains its time stamp by reading the current value of the event receiver's time stamp counter. This mode causes a VME access each time the record is processed and so should be used judiciously. As an aside, in the absence of an event receiver, EPICS uses NTP to synchronize timestamps across multiple processors. It's been our experience that timestamps are synchronized to no better than 100ms across multiple processors when the EPICS NTP is used.

We plan to use the high resolution time stamps to help unfold the sequence of hardware trips that may occur when beam is lost. A likely scenario is that an initiating occurrence will cause beam to be lost and also cause a cascade of trips. EPICS monitors all trip sources. Inspection of the high resolution time stamps should help determine the failure sequence.

## SUMMARY

The APS Event Timing System has been in production use for nearly two years. We have found it to be extremely useful for generating timing outputs at distributed locations. The ability to trigger EPICS record processing upon occurrence of a timing event has been extremely useful.

## REFERENCES

- [1] Advanced Micro Devices, Inc., Am7968/AM7969 TAXIchip Handbook, Publication BAN-13.5M-5/94-0, Sunnyvale, CA, April 7, 1994

## DISCLAIMER

This report was prepared as an account of work sponsored by an agency of the United States Government. Neither the United States Government nor any agency thereof, nor any of their employees, makes any warranty, express or implied, or assumes any legal liability or responsibility for the accuracy, completeness, or usefulness of any information, apparatus, product, or process disclosed, or represents that its use would not infringe privately owned rights. Reference herein to any specific commercial product, process, or service by trade name, trademark, manufacturer, or otherwise does not necessarily constitute or imply its endorsement, recommendation, or favoring by the United States Government or any agency thereof. The views and opinions of authors expressed herein do not necessarily state or reflect those of the United States Government or any agency thereof.

with 600 germanium crystals arranged in 8 rings. Figure 4 shows schematic drawing of

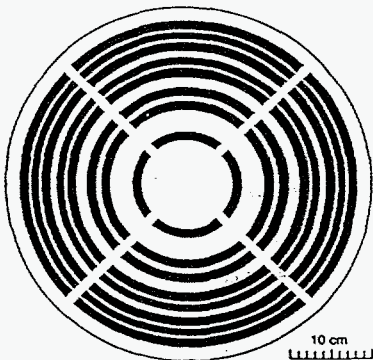


Figure 4. Schematic drawing of the crystal lens with outer dia. of 90 cm

this lens with its 8 rings of crystal cubes. Each crystal cube was mounted on an aluminum plate, one end of which was bolted to the lens frame and the other end was free to move. The diffraction angle of each crystal was adjusted separately by applying a light force on the free end of the aluminum plate through a soft spring. This resulted in a slight bending of the plate and allowed one to adjust each crystal so that the appropriate crystalline planes make the right Bragg angle ( $\pm 5$  arc sec) with the incident radiation to satisfy the required relation,  $\lambda = 2d \sin\theta$ . A  $^{137}\text{Cs}$  source of 661.65 keV was used to align the individual crystals, one at a time. Seven different gamma-ray energies have been used in the tests with this lens system. They are listed in Table I, with their source, full lens focal lengths, and distances from source to lens and lens to detector. All of these measurement were made without retuning the lens. All that was needed to focus a new energy was to change the distance from the source to the lens and place the detector at the new focal point as explained above.

Energy (keV)	Source	Focal Length (meters)	Source-Lens (meters)	Lens-detector (meters)
661.65	$^{137}\text{Cs}$	10.92	24.75	19.54
511.00	$^{22}\text{Na}$	8.43	19.11	15.09
413.7	$^{239}\text{Pu}$	6.83	15.47	12.22
383.71	$^{133}\text{Ba}$	6.33	14.35	11.33
375.2	$^{239}\text{Pu}$	6.19	14.03	11.08
355.94	$^{133}\text{Ba}$	5.87	13.31	10.51
302.83	$^{133}\text{Ba}$	5.00	11.33	9.70

Table 1: Gamma-ray sources tested with ANL germanium crystal lens.

### 3. CRYSTAL DIFFRACTION FORMULA

The crystal diffraction angle  $\theta_B$  is defined by equations:

$$\sin\theta_B = n\lambda / 2d \quad (1)$$

and

$$\lambda(A) = 12.397 / E_\gamma (\text{keV}) \quad (2)$$

where  $\lambda$  is the wavelength of the gamma-ray (in Angstrom units in eq. 2),  $d$  is the crystalline spacing,  $n$  is the order of the diffraction, and  $E_\gamma$  is the energy of the gamma-ray, in keV. For a 100 keV gamma-ray, diffracted by the [111] planes of germanium,  $\theta_B$  is about 1.0895 degrees, 0.01902 radians. Thus the surface of a Bragg diffraction crystal

will need to be 52.6 times longer than the height of a Laue crystal used to diffract the same size beam. (see figure 2)

Each ring uses a different set of crystalline planes and can be of different crystalline material as well. The focal length (F.L.) for each ring (the distance from the ring to the focus for a distant source) is given by equation 3,

$$F.L. = R / \tan 2\theta \quad (3)$$

where  $R$  is the radius of the ring and  $\theta$  is the Bragg diffraction angle defined above. By adjusting  $R$  one can make the focal lengths of all the rings the same and obtain a single focus for the full lens. Substituting equations 1 & 2 in 3

$$F.L. = R / \tan (2 \arcsin [(12.397) n / 2d E_Y]) \quad (4)$$

For small Bragg angles

$$F.L. = [R ((12.397) n d(A)) E_Y] / (keV) \quad (5)$$

so for any ring with a given  $R$  and  $d$ ,

$$F.L. = \text{constant} \times E_Y \quad (6)$$

If all of the rings have the same focal length, then eq. 6 is true for the full lens.

For a source at a finite distance from the lens, eq. 7 and 8 must be satisfied along with eq. 1 & 2.

$$L_S = R / \tan(\theta - \alpha) \quad (7)$$

$$L_D = R / \tan(\theta + \alpha) \quad (8)$$

where  $L_S$  is the distance from the source to the lens,  $L_D$  is the distance from the lens to the detector, and  $\alpha$  is the angle between the crystalline planes and the axis of the lens. For the case of a distant source  $\alpha = q$ . The small angle approach gives:

$$F.L. = 1/F_S + 1/L_D \quad (9)$$

which is the simple lens formula for a simple convex lens with visible light.

A typical scan over a small source ( $^{137}\text{Cs}$ ) is shown in Figure 3. The background count rate is very small, less than 0.1 counts per sec., so the wings are a real part of the scan. These wings come about because the view of a single crystal is not a small circular (angular) area of space but rather a strip across the sky. This strip is narrow in the diffraction plane but can be quite wide in the plane perpendicular to the diffraction plane. This wide angular width depends on, the width of the individual crystals, the width of the

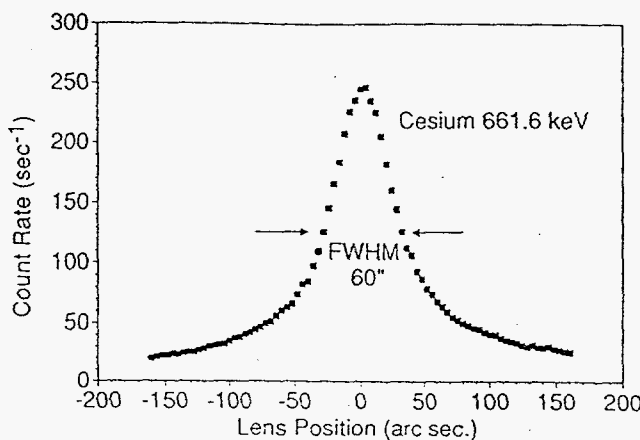


Figure 5. Vertical scan of crystal lens over a 3 mm dia.  $^{137}\text{Cs}$  source.

detector and the distance from the lens to the detector. If the crystal is 2-cm wide; the detector 6-cm wide; and the distance from lens to detector is 800 cm, then the angular width of the strip of the sky viewed by the crystal is 0.01 radians, which is 2063 arc seconds or 34.37 arc min. The wide wings seen in figure 5 would extend out either side of the peak by 1032 arc sec.

#### 4. Off-Axis Response

The wide wings in the field of view give the lens considerable off-axis sensitivity and make it much easier to locate a source. They also contribute significantly to the sensitivity (count rate) of the lens when the source has a finite angular size. For an extended source the wings can contribute more to the count rate in the detector than the central region of the field of view. This is because, although the sensitivity of the lens to off-axis sources decreases with the angular distance off-axis, the area being viewed increases at about the same rate. Thus each angular ring of the source contributes the same amount of focused flux to the diffracted beam. If the source exhibits a continuum energy spectrum, then a more complicated picture emerges. The corresponding view for an individual crystal for wavelengths other than that for which the lens focus was adjusted, will still be a strip of the sky but now it will be displaced from the center of the field of view. The strength of this response is strongest from a ring surrounding the center of the field of view. If the source is an extended source, then this wavelength will be focused on the detector as a ring surrounding the center of the detector and a series of wavelengths will be focused on the detector as a series of rings. If the source has an irregular shape, this shape will be imaged on the detector. If a monochromatic source is off center to the left, its image at the focal point will be off center to the right. Thus, the crystal lens has many of the features of a simple convex lens for visible light. This discussion suggests that a multi-element detector would be quite useful at the focal point of the lens, both for locating the source and for determining its size and shape. Just such an experiment was performed at Argonne using a multi-element Ge detector supplied by the astrophysics group from Toulouse. This collaborative (Argonne + Toulouse) experiment is described in another paper presented at this meeting.

#### 5. Angular Resolution and Diffraction Efficiency

The angular resolution and the diffraction efficiency both depend on the physical properties of the crystals, alignment errors of the crystals, and on the design of the lens. These components are strongly coupled. Lenses that have good angular resolution tend to have good energy resolution, high diffraction efficiencies, large effective areas and low backgrounds for a narrow band width of gamma-ray energies. While lenses that are designed to focus large energy bandwidths tend to have poor angular resolution, smaller effective areas, and lower diffraction efficiencies for gamma-ray sources with narrow bandwidths. The full Argonne lens contains 600 germanium crystals in the form of 1 cm cubes, mounted in 8 rings. The diffraction planes used and the number of crystals in each ring are, respectively: [111], 28; [220], 52; [311], 60; [400], 76; [331], 84; [422], 92; [333], 100; [440], 108. They are all used in Laue (transmission) diffraction and have mosaic structures that are much larger than their Darwin widths. For a simple unbent crystal cube, the diffraction efficiency (the number of gamma rays focused on the detector divided by the number of gamma rays incident on the crystal) is the product of the transmission of the gamma rays through the crystal times the diffraction coefficient for the crystalline planes and is given by equation 11,

$$\text{Diff. Eff.} = (\exp -\alpha x) [0.5 (1 - \exp \alpha x)] \quad (11)$$

where  $\alpha$  is linear absorption coefficient;  $\sigma$  is the linear diffraction coefficient; and  $x$  is the thickness of the Laue crystal. For the 661.65-keV line from  $^{137}\text{Cs}$ , the transmission is 70% for a 1 cm germanium crystal and the maximum diffraction coefficient is 50%, giving 35% for the maximum efficiency. The individual crystals have diffraction efficiencies for

the Cs line that range from 4% to 15%, depending on their mosaic structure and the crystalline planes used. These low efficiencies result from the use of crystals that are too perfect. The average acceptance angle of these crystals is 2 arc sec. The 3-mm dia. Cs source intercepts an angle of 25 arc sec as seen from the lens and the 1-cm crystals intercept an angle of 82 arc sec as seen from the source. Both of these subtended angles are much larger than the acceptance angle of the crystals so only a small region of the crystal can diffract gamma rays from a point in the source, and only a fraction of the crystal can diffract gamma rays from any part of the source. If these geometric effects are combined with the equation 11, they would predict that the diffraction efficiency of the lens would be less than 1 percent and its performance, very poor. The increase in the efficiency was obtained by cutting slots in the back of each crystal and wedging the three sectors apart so they made a 27-arc-sec angle with their adjacent sections. This reduced the miss match between the acceptance angles and the size of the crystals and the size of the source. Further improvements in the efficiency of the crystals was made by roughing the surfaces of the crystal. This increased the mosaic structure of small regions of the crystals near the surfaces. The net effect was to improve the efficiency from less than 1 percent to the 4 to 15 percent mentioned above.

Table II gives the diffraction efficiencies with the present lens for the measured sources, normalized to a constant distance from the source to the lens of 24.75 m and a constant diameter source, 3-mm dia., (25 arc sec). The last column gives the effective area of the full lens at that energy.

Energy (keV)	Element	Diffraction Efficiency	Eff. Area, cm <sup>2</sup>
661.65	137 Cs	0.070	39.
551.00	22 Na	0.14	78.
413.7	239 Pu	0.22	123.
383.7	133 Ba	0.25	140.
355.9	133 Ba	0.27	151.
302.8	133 Ba	0.24	134.

Table 2: Diffraction efficiencies and effective areas for the 45 cm Lens

If the present crystals are replaced with crystals that have the optimum mosaic structure widths and the optimum thickness, the projected diffraction efficiency will be 25 to 40 % for these gamma-ray energies. This corresponds to an effective area of 150 to 240 cm<sup>2</sup>. A lens with an effective area of this size should be quite acceptable for a balloon experiment. In all of these experiments, the direct beam from the source to the detector is blocked. If the central region of the lens is opened up so that the detector can see the source, then the effective areas will increase by the area of the detector (28 cm<sup>2</sup>).

The width of the scan over the Cs source (60 arc sec), as shown in Figure 3, is due to the width of the source (25 arc sec), the size of the 3 subsections (25 arc sec) of each crystal and the 1.6 size increase in width that comes from the circular geometry of the lens. The calculated width, 57 arc sec, is close to the measured value of 60 arc sec. Relatively little of the width is due to the misalignment of the crystals.

## 6. Standard and Multi-Element Detectors

The Argonne lens system was tested with a standard intrinsic-germanium gamma-ray detector and also with a 3 x 3 matrix of germanium detectors brought to Argonne by

the astrophysics group from Toulouse.<sup>8</sup> More detail on the test results of this lens / matrix-detector combination can be found in the paper presented by Juan Naya at this conference.

## 7. Tunable Crystal Lens

The major advantage of the Argonne-type lens that adjusts all of the crystals to focus a narrow band of wavelengths and thus maximize its sensitivity for that wavelength, is also a major drawback for some experiments. Concentrating on one gamma-ray energy is all right for a balloon experiment, where the observation time is limited but it would not be acceptable for a satellite experiment, where one would like to view many different wavelengths. This means that one must be able to retune the lens to a new wavelength. The Toulouse - Argonne collaboration has devised at least two different ways of accomplishing this. Details on how this can be accomplished can found in a paper presented at this conference by Peter von Ballmoos.<sup>10</sup>

### Acknowledgement

This work was supported in part by the DOE contract No. W31-109-88-~~ENG~~. The germanium crystal lens was designed and built with funds supplied by the DOE Office of Nonproliferation and National Security for the work preformed at ANL for the project entitled "Crystal Diffraction Lens For Long-Range Passive Detection Of Fissile Material".

### References:

1. "New Method for Focusing X-Rays and Gamma-Rays", R.K. Smither, Rev. Sci. Instrum., 44, 131-141 (Feb. 1982).
2. "New Method for Focusing and Imaging X-Rays and Gamma-Rays with Diffraction Crystals", R. K. Smither, Sym. on Future X-Ray Experiments, X-Rays in the 80's, GSFC, Oct. 1981, NASA Tech. Mem. No. 83848 (Nov. 1981)
3. "A Positron Annihilation Radiation Telescope Using Laue Diffraction in a Crystal Lens", R. K. Smither and Peter von Ballmoos, INTEGRAL Workshop, Feb. 2-5 at Les Diablerets, Switzerland. AP supp., Vol. 92, 1994 June, 663
4. "A Bragg Crystal Flux Concentrator for Annihilation Radiation", R.K. Smither and N. Lund, 16th Inter. Cosmic Ray Conference, India (1983). Conference proceedings, supplement issue of AP.
5. "Crystal Diffraction Telescope for Discrete line sources", R.K. Smither, et. al., GRO Science Workshop, GSFC, April 1989, NASA Report, Ed. W. Neil Johnson.
6. "A Study of Focusing Telescopes for Soft Gamma Rays", Niels Lund, Experimental Astronomy Vol 2, (1992) 259
7. "Gamma-Ray Telescopes Using Variable-Metric Diffraction Crystals", R.K. Smither, 11th Texas Symposium on Relativistic Astrophysics", Austin, Texas, Dec. 1981, Annal. of New York Acad. Sci., 422 (1983) 384
8. "Crystal Diffraction Lenses for Imaging Gamma-Ray Telescope", R.K. Smither, "13th Texas Symposium on Relativistic Astrophysics," p 55-59, Ed. M.P. Ulmer, Northwestern Un., World Scientific Publishing Co., Singapore
9. "Experimental Results Obtained with the Positron-AnnihilationRadiation Telescope of the Toulouse-Argonne Collaboration", Juan Naya, et. al., contributed paper No. of this conference, p
10. "A Space Borne Crystal Diffraction Telescope for the Energy range of Nuclear Transitions", Peter von Ballmoos, et. al., contributed paper No. " " of this conference.